A Tension Approach to Controlling the Shape of Cubic Spline Surfaces on FVS Triangulations

Oleg Davydov* and Carla Manni†

January 8, 2009

Abstract

We propose a parametric tensioned version of the FVS macro-element to control the shape of the composite surface and remove artificial oscillations, bumps and other undesired behaviour. In particular, this approach is applied to C^1 cubic spline surfaces over a four-directional mesh produced by two-stage scattered data fitting methods.

Keywords: Tension, Bivariate Splines, Two-stage scattered data fitting
Classification codes (MSC2000): 41A15, 41A63, 65D07, 65D15, 65D17

1 Introduction

Interpolating or approximating schemes which guarantee the preservation of salient properties (monotonicity, convexity, etc.) of the data are of a great interest in several applications and have received a considerable attention in the last decades. They are usually referred to as *shape preserving* schemes, see [17] and references therein.

Piecewise polynomials are among the most popular functions in interpolation and approximation of given data sets but they often present undesired oscillations and bumps extraneous to the behavior of the data, that is they are not shape-preserving.

In order to obtain shape-preserving schemes, polynomials are usually replaced by spaces of functions (exponentials, rationals, variable degree polynomials, etc.) depending on some *shape parameters* (see for example [2], [10], [11], [19], [20], [24] and references quoted therein). Intermediate values of the shape parameters give rise to smooth approximations intermediate between the spline and a piecewise linear or bilinear function. Due to this, the above mentioned methods are often called *tension methods* and the related shape parameters *tension parameters*.

Among tension methods, we recall the *parametric approach*, see [22, 5, 23] and references therein, where the approximating function (more precisely, its graph) is given by a a particular parametric curve or surface whose components belong to simple polynomial spline spaces, such as piecewise quadratics or cubics. The amplitude of the tangent vectors at salient points play the role of the tension parameters.

Cubic FVS macro-elements are based on a quadrangulation with two diagonals drawn into each quadrilateral, and have certain advantages over other well known macro-elements like Powell-Sabin quadratics and Clough-Tocher cubics, see [21].

*Department of Mathematics, University of Strathclyde, 26 Richmond Street, Glasgow G1 1XH, Scotland
†Department of Mathematics, University of Rome "Tor Vergata", Via della Ricerca Scientifica, 00133, Roma, Italy.

In this paper we use the parametric approach to produce a new shape-preserving scheme based on the FVS cubic element and illustrate its performance by an application to scattered data fitting, where substantial reduction of small scale artefacts in a cubic spline surface computed by a two-stage method of [8] is achieved by an automatic procedure for the selection of tension parameters.

The paper is organized as follows. In Section 2 we recall the definition of the FVS triangulation and construction of C^1 cubic FVS macro-elements and corresponding splines. The details of the parametric tension approach applied to these splines are presented in Section 3, while Section 4 is devoted to the conditions that need to be satisfied by the tension parameters in order to ensure the shape preserving properties, such as monotonicity and/or convexity along the edges of the quadrangulation. Section 5 presents an example application to scattered data fitting. Finally, a conclusion is given in Section 6.

2 Cubic splines on FVS triangulations

Let $\Omega \subset \mathbb{R}^2$ be a polygonal domain, and $\square$ a quadrangulation of it, where each quadrilateral $Q \in \square$ is strictly convex. Let $\mathcal{V}$ and $\mathcal{E}$ denote the sets of all vertices and edges of $\square$, respectively.

By drawing in the diagonals of each $Q \in \square$ we obtain a triangulation denoted $\boxtimes$. We say that $\boxtimes$ is an *FVS triangulation* of Ω.

We denote by $S_3^1(\boxtimes)$ the space of all C^1 cubic splines on $\boxtimes$,

$$S_3^1(\boxtimes) = \{s \in C^1(\Omega) \,:\, s|_T \in \Pi_3 \ \text{ for all } \ T \in \boxtimes\},$$

where Π_3 is the space of all polynomials of total degree at most 3. We will refer to $S_3^1(\boxtimes)$ as the space of *FVS splines*.

The space $S_3^1(\boxtimes)$ has a particularly simple structure because its restrictions on the quadrilaterals $Q \in \square$ are the spaces of *FVS macro-elements* described by Fraeijs de Veubeke [12] and Sander [16], see also [21, Section 6.5].

The dimension of $s \in S_3^1(\boxtimes)$ is given by the formula $3V + E$, where $V = \#\mathcal{V}$, $E = \#\mathcal{E}$, and every $s \in S_3^1(\boxtimes)$ is completely determined by its function and gradient values at the vertices of $\square$,

$$f_{\mathbf{v}} = s(\mathbf{v}), \quad \nabla f_{\mathbf{v}} = \nabla s(\mathbf{v}), \qquad \mathbf{v} \in \mathcal{V}, \tag{2.1}$$

and the normal derivatives at the midpoints of the edges of $\square$.

In particular, every quadrilateral patch $s|_Q$, $Q = [\mathbf{v}_1, \mathbf{v}_2, \mathbf{v}_3, \mathbf{v}_4] \in \square$ is uniquely determined by the data

$$f_{\mathbf{v}_i}, \quad \nabla f_{\mathbf{v}_i}, \qquad i = 1, 2, 3, 4, \tag{2.2}$$

and the four normal derivatives at $(\mathbf{v}_i + \mathbf{v}_{i+1})/2$, $i = 1, 2, 3, 4$ ($\mathbf{v}_5 := \mathbf{v}_1$), as depicted in Fig. 1 (left).

Alternatively, $s|_Q$ can be described by its Bézier net. Let T_ℓ denote the triangle $[\mathbf{v}_\ell, \mathbf{v}_{\ell+1}, \mathbf{w}] \in \boxtimes$, $\ell = 1, 2, 3, 4$, where $\mathbf{w}$ is the intersection point of the diagonals of Q. Each triangle patch $s|_{T_\ell}$ is a cubic polynomials and can be expanded as a linear combination of cubic Bernstein basis polynomials, i.e.,

$$s|_{T_\ell} = \sum_{\mathbf{t} \in \mathcal{D}_{T_\ell}} c_{\mathbf{t}} B_{\mathbf{t}}^{T_\ell}, \qquad c_{\mathbf{t}} \in \mathbb{R},$$

where

$$\mathcal{D}_{T_\ell} := \left\{ \mathbf{t}_{ijk}^{T_\ell} = \frac{i\mathbf{v}_\ell + j\mathbf{v}_{\ell+1} + k\mathbf{w}}{3} \right\}_{i+j+k=3}$$

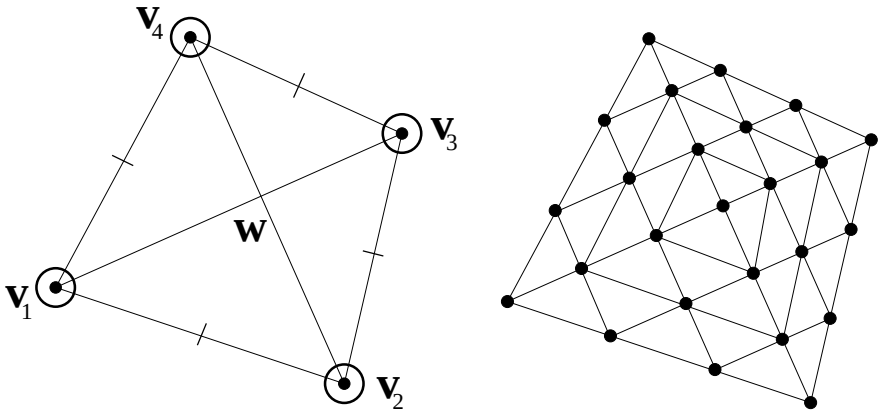

Figure 1: Left: Degrees of freedom of a FVS macro element. The dots and circles at the vertices depict function values and gradients, respectively. The dashes at the middle points of the edges depict normal derivatives. Right: domain points in $\mathcal{D}_Q$.

and

$$B_{\mathbf{t}}^{T_\ell} = B_{ijk}^{T_\ell} = \frac{3!}{i!j!k!} b_1^i b_2^j b_3^k \qquad \text{if} \quad \mathbf{t} = \mathbf{t}_{ijk},$$

with b_1, b_2, b_3 being the barycentric coordinates with respect to T_ℓ. We also write $c_{\mathbf{t}} = c_{ijk}^{T_\ell}$ if $\mathbf{t} = \mathbf{t}_{ijk}^{T_\ell}$

The elements of the sets $\mathcal{D}_{T_\ell}$ are called *domain points*, and we denote the unions of these sets as follows

$$\mathcal{D}_Q := \mathcal{D}_{T_1} \cup \mathcal{D}_{T_2} \cup \mathcal{D}_{T_3} \cup \mathcal{D}_{T_4}, \qquad \mathcal{D}_{\boxtimes} := \bigcup_{Q \in \boxtimes} \mathcal{D}_Q.$$

The set $\mathcal{D}_Q$ is illustrated in Fig. 1 (right). Since any $s \in S_3^1(\boxtimes)$ is continuous, the coefficient $c_{\mathbf{t}}$ of s is uniquely defined for any $\mathbf{t}$ lying on common edges of different triangles in $\boxtimes$. Therefore s is uniquely represented by its sequence of coefficients $\{c_{\mathbf{t}} : \mathbf{t} \in \mathcal{D}_{\boxtimes}\}$. The points

$$\mathbf{C}_{\mathbf{t}} = (\mathbf{t}, c_{\mathbf{t}}) \in \mathbb{R}^3, \qquad \mathbf{t} \in \mathcal{D}_{\boxtimes},$$

are called *control points* of the spline. By connecting the control points along edges shown in Fig. 1 (right), a wireframe object called *Bézier net* is obtained. In fact, any sequence of coefficients $\{c_{\mathbf{t}} \in \mathbb{R} : \mathbf{t} \in \mathcal{D}_{\boxtimes}\}$ generates a Bézier net of a *continuous* piecewise cubic spline s. In order for s to lie in $S_3^1(\boxtimes)$, the Bézier net must satisfy Farin's *smoothness conditions* saying that certain groups of control points belong to the same plane. Namely, these are:

1) for any vertex $\mathbf{v}$ of $\boxtimes$, the control point corresponding to the domain point at $\mathbf{v}$ and all control points connected to it in the Bézier net,

2) for any interior edge of $\boxtimes$, two middle control points on that edge, and the interior points of two triangles sharing the edge.

3 Parametric tension

The splines $s \in S_3^1(\boxtimes)$ can be interpreted as parametric surfaces

$$\mathbf{S}(x, y) = (x, y, s(x, y))^T. \tag{3.1}$$

Since x and y are linear functions, they are in the space $S_3^1(\boxtimes)$, and hence possess their own coefficients $c_{\mathbf{t}}^x$, $c_{\mathbf{t}}^y$, $\mathbf{t} \in \mathcal{D}_{\boxtimes}$ with respect to the Bernstein basis polynomials.

The parametric approach consists in introducing certain parameters in the parametric surface $\mathbf{S}$, see [23]. More precisely, let $\Lambda = \{\lambda_{\mathbf{v}}\}_{\mathbf{v}\in\mathcal{V}}$ be a sequence of *tension parameters* satisfying $\lambda_{\mathbf{v}} \in [0,1]$. Given a spline $s \in S_3^1(\boxtimes)$, we define a parametric surface called *tensioned FVS spline*

$$\mathbf{S}^\Lambda(x,y) = (X^\Lambda(x,y), Y^\Lambda(x,y), Z^\Lambda(x,y))^T, \qquad (x,y)\in\Omega,$$

as follows. Let Q be a quadrilateral in $\square$, and let $T_\ell := [\mathbf{v}_\ell, \mathbf{v}_{\ell+1}, \mathbf{w}] \in \boxtimes$, $\ell = 1,2,3,4$, be the subtriangles of $\square$ as in Section 2. We denote by $\mathbf{e}_\ell$ the edge $\mathbf{v}_{\ell+1} - \mathbf{v}_\ell$. For each ℓ, $\mathbf{S}^\Lambda|_{T^\ell}$ is a parametric Bézier surface defined by

$$\mathbf{S}^\Lambda|_{T^\ell} := \sum_{\mathbf{t}\in\mathcal{D}_{T_\ell}} \mathbf{C}_{\mathbf{t}}^\Lambda B_{\mathbf{t}}^{T_\ell}, \tag{3.2}$$

where $\mathbf{C}_{\mathbf{t}}^\Lambda = \mathbf{C}_{ijk}^{T^\ell} = \mathbf{C}_{ijk}^{T^\ell}(\lambda_{\mathbf{v}_1}, \lambda_{\mathbf{v}_2}, \lambda_{\mathbf{v}_3}, \lambda_{\mathbf{v}_4})$ if $\mathbf{t} = \mathbf{t}_{ijk}^{T^\ell}$, with

$$\mathbf{C}_{300}^{T^\ell} = \begin{pmatrix} \mathbf{v}_\ell \\ f_{\mathbf{v}_\ell} \end{pmatrix}, \tag{3.3}$$

$$\mathbf{C}_{030}^{T^\ell} = \begin{pmatrix} \mathbf{v}_{\ell+1} \\ f_{\mathbf{v}_{\ell+1}} \end{pmatrix}, \tag{3.4}$$

$$\mathbf{C}_{210}^{T^\ell} = \mathbf{C}_{300}^{T^\ell} + \frac{\lambda_{\mathbf{v}_\ell}}{3}\begin{pmatrix} \mathbf{e}_\ell \\ \langle \nabla f_{\mathbf{v}_\ell}, \mathbf{e}_\ell\rangle \end{pmatrix}, \tag{3.5}$$

$$\mathbf{C}_{120}^{T^\ell} = \mathbf{C}_{030}^{T^\ell} - \frac{\lambda_{\mathbf{v}_{\ell+1}}}{3}\begin{pmatrix} \mathbf{e}_\ell \\ \langle \nabla f_{\mathbf{v}_{\ell+1}}, \mathbf{e}_\ell\rangle \end{pmatrix}, \tag{3.6}$$

$$\mathbf{C}_{201}^{T^\ell} = \mathbf{C}_{300}^{T^\ell} + \frac{\lambda_{\mathbf{v}_\ell}}{3}\begin{pmatrix} \mathbf{w}-\mathbf{v}_\ell \\ \langle \nabla f_{\mathbf{v}_\ell}, \mathbf{w}-\mathbf{v}_\ell\rangle \end{pmatrix}, \tag{3.7}$$

$$\mathbf{C}_{021}^{T^\ell} = \mathbf{C}_{030}^{T^\ell} + \frac{\lambda_{\mathbf{v}_{\ell+1}}}{3}\begin{pmatrix} \mathbf{w}-\mathbf{v}_{\ell+1} \\ \langle \nabla f_{\mathbf{v}_{\ell+1}}, \mathbf{w}-\mathbf{v}_{\ell+1}\rangle \end{pmatrix}. \tag{3.8}$$

In addition, $\mathbf{C}_{111}^{T^\ell}$ is determined so that

$$\frac{\partial \mathbf{S}^\Lambda|_{T^\ell}}{\partial \mathbf{n}_\ell}\left(\frac{\mathbf{v}_\ell + \mathbf{v}_{\ell+1}}{2}\right) = \frac{\lambda_{\mathbf{v}_\ell} + \lambda_{\mathbf{v}_{\ell+1}}}{2}\begin{pmatrix} \mathbf{n}_\ell \\ \frac{\partial f}{\partial \mathbf{n}_\ell}\left(\frac{\mathbf{v}_\ell+\mathbf{v}_{\ell+1}}{2}\right)\end{pmatrix}, \tag{3.9}$$

where $\mathbf{n}_\ell$ denotes the normal to the edge $\mathbf{e}_\ell$. Finally, the remaining Bézier control points $\mathbf{C}_{102}^{T^\ell}, \mathbf{C}_{012}^{T^\ell}, \mathbf{C}_{003}^{T^\ell}$ are determined so as to ensure the C^1 continuity of each component of $\mathbf{S}^\Lambda|_Q$ across the edges $\mathbf{w}-\mathbf{v}_\ell$, $\ell = 1,2,3,4$.

An alternative interpretation of the above conditions is that each of $X^\Lambda(x,y)$, $Y^\Lambda(x,y)$ and $Z^\Lambda(x,y)$ is a spline in $S_3^1(\boxtimes)$ that interpolates some suitable data. For example, X^Λ satisfies the following interpolation conditions

$$X^\Lambda(\mathbf{v}) = \mathbf{v}^x, \quad \nabla X^\Lambda(\mathbf{v}) = (\lambda_{\mathbf{v}}, 0)^T, \qquad \mathbf{v}\in\mathcal{V},$$

$$\frac{\partial X^\Lambda}{\partial \mathbf{n}_{\mathbf{e}}}\Big(\mathbf{m}_{\mathbf{e}}\Big) = \tfrac{\lambda_{\mathbf{v}_\ell}+\lambda_{\mathbf{v}_{\ell+1}}}{2}\mathbf{n}_{\mathbf{e}}^x, \qquad \mathbf{e}\in\mathcal{E},$$

where $\mathbf{n}_{\mathbf{e}}$ denotes the normal to the edge $\mathbf{e}$, $\mathbf{m}_{\mathbf{e}}$ its midpoint, and $\mathbf{v}^x, \mathbf{n}_{\mathbf{e}}^x$ the x-components of the vectors $\mathbf{v}$ and $\mathbf{n}_{\mathbf{e}}$, respectively.

From the above construction, for all $\lambda_{\mathbf{v}} \in [0,1]$ the components X^Λ, Y^Λ and Z^Λ of $\mathbf{S}^\Lambda$ are C^1 functions on Ω.

Given $Q \in \square$, it is clear that the quadrilateral patch $\mathbf{S}^\Lambda|_Q$ depends only on four tension parameters $\lambda_{\mathbf{v}}$ assigned to the vertices $\mathbf{v}_1, \mathbf{v}_2, \mathbf{v}_3, \mathbf{v}_4$ of Q. We set

$$\mathbf{S}_Q = \mathbf{S}_Q^{(\lambda_1,\lambda_2,\lambda_3,\lambda_4)} := \mathbf{S}^\Lambda|_Q, \qquad Q \in \square,$$

where $\lambda_\ell = \lambda_{\mathbf{v}_\ell}$, $\ell = 1, 2, 3, 4$. We refer to $\mathbf{S}_Q$ as *tensioned FVS macro-element*. We will also need the componentwise notation for $\mathbf{S}_Q$,

$$\mathbf{S}_Q = (X_Q, Y_Q, Z_Q)^T = (X_Q^{(\lambda_1,\lambda_2,\lambda_3,\lambda_4)}, Y_Q^{(\lambda_1,\lambda_2,\lambda_3,\lambda_4)}, Z_Q^{(\lambda_1,\lambda_2,\lambda_3,\lambda_4)})^T. \tag{3.10}$$

From (3.3)–(3.9) it is easy to see that $\mathbf{S}_Q^{(1,1,1,1)} = \mathbf{S}|_Q$, where $\mathbf{S}$ is the parametric surface that represents $s \in S_3^1(\boxtimes)$, as defined in (3.1). On the other hand, if $\lambda_1 = \lambda_2 = \lambda_3 = \lambda_4 = 0$, the Bézier control points

$$\mathbf{C}_{i,j,k}^{T^\ell}(0,0,0,0), \quad k = 0, 1, \quad \ell = 1, 2, 3, 4,$$

belong to the straight line in $\mathbb{R}^3$ through $(\mathbf{v}_\ell, f_{\mathbf{v}_\ell})$ and $(\mathbf{v}_{\ell+1}, f_{\mathbf{v}_{\ell+1}})$, while, from the C^1 continuity conditions, the remaining Bézier control points are convex combinations of them. Thus, the following statement follows from the convex hull property of the Bézier-Bernstein representation.

Proposition 3.1. *The graph of $\mathbf{S}_Q^{(0,0,0,0)}$ is contained in the convex hull of the four control points $\mathbf{C}_{\mathbf{v}_\ell} = (\mathbf{v}_\ell, f_{\mathbf{v}_\ell})^T$, $\ell = 1, 2, 3, 4$, of the original spline s. Moreover, it includes the straight line segments $[\mathbf{C}_{\mathbf{v}_\ell}, \mathbf{C}_{\mathbf{v}_{\ell+1}}]$, $\ell = 1, 2, 3, 4$.*

In particular, if the control points $\mathbf{C}_{\mathbf{v}_\ell}$, $\ell = 1, 2, 3, 4$, lie on one plane, then the graph of $\mathbf{S}_Q^{(0,0,0,0)}$ coincides with this plane. Note that this surface resembles the behaviour of the bilinear interpolant, see Fig. 2 (bottom).

Summarizing, the parameters $\lambda_1, \lambda_2, \lambda_3, \lambda_4$ act as tension parameters on the graph of the surface patch $\mathbf{S}_Q$, stretching it from the classical FVS macro-element to a "straightened" surface interpolating the data positions and reducing to an affine function along the edges of Q, see Fig. 2.

We now turn to the question of whether the surface $\mathbf{S}_Q$ represents the graph of a function $z = s_Q(x, y)$. To this end we consider the transformation $\mathbf{T}_Q = \mathbf{T}_Q^{(\lambda_1,\lambda_2,\lambda_3,\lambda_4)} : Q \to \mathbb{R}^2$ defined by the first two components of $\mathbf{S}_Q$,

$$\mathbf{T}_Q(x, y) := (X_Q(x, y), Y_Q(x, y))^T. \tag{3.11}$$

Clearly, $\mathbf{S}_Q$ is the graph of a function defined on Q if and only if $\mathbf{T}_Q$ is a one-to-one mapping of Q.

Proposition 3.2. *The transformation $\mathbf{T}_Q$ is one-to-one on the boundary of Q for any $\lambda_\ell \in [0, 1]$, $\ell = 1, 2, 3, 4$. Moreover, $\mathbf{T}_Q(Q) = Q$, $\mathbf{T}_Q(\mathbf{v}_\ell) = \mathbf{v}_\ell$, $\ell = 1, 2, 3, 4$, and the Jacobian $J(\mathbf{T}_Q)$ of $\mathbf{T}_Q$ at $\mathbf{v}_\ell$ is given by*

$$J(\mathbf{T}_Q)(\mathbf{v}_\ell) = \begin{bmatrix} \lambda_\ell & 0 \\ 0 & \lambda_\ell \end{bmatrix}.$$

Proof. From (3.3)–(3.9), $\mathbf{T}_Q|_{\mathbf{e}_\ell}$ is a plane cubic Bézier curve with control points $\mathbf{v}_\ell$, $\mathbf{v}_\ell + \frac{\lambda_\ell}{3}\mathbf{e}_\ell$, $\mathbf{v}_{\ell+1} - \frac{\lambda_\ell}{3}\mathbf{e}_\ell$, $\mathbf{v}_{\ell+1}$, all on the edge $\mathbf{e}_\ell$. By the convex hull property of Bézier curves it follows that $\mathbf{T}_Q(\mathbf{e}_\ell) = \mathbf{e}_\ell$. Moreover, it is easy to see that the curve has its endpoints at $\mathbf{v}_\ell$ and $\mathbf{v}_{\ell+1}$, and its parametrisation is strictly monotone everywhere in the interior of the interval

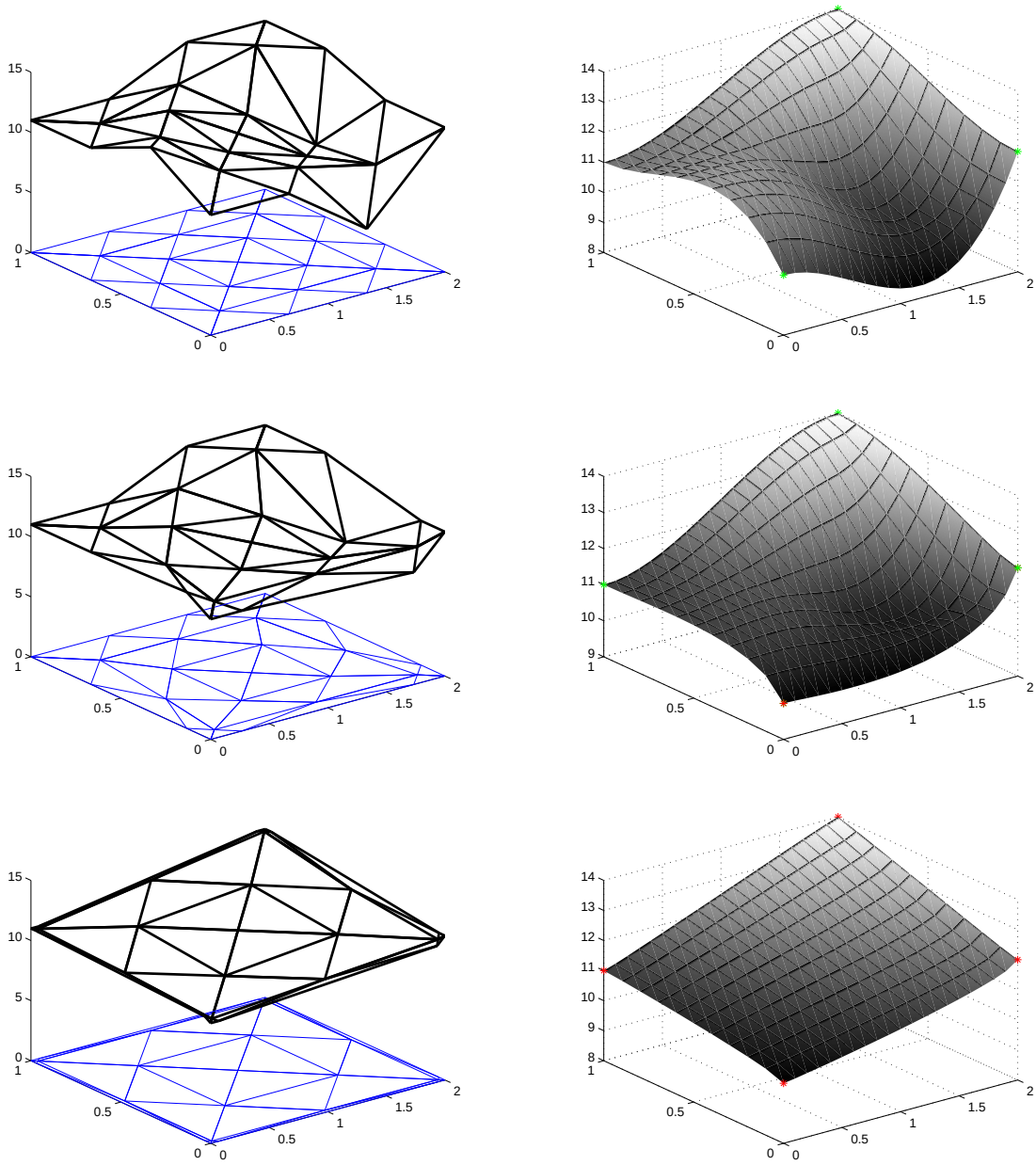

Figure 2: Left: Bézier net of $\mathbf{S}_Q$ and its projection on the x, y plane (i.e. Bézier net of $\mathbf{T}_Q$). Right: graph of s_Q. Top: $\lambda_\ell = 1,\ \ell = 1, 2, 3, 4$. Center: $\lambda_\ell = .4,\ \ell = 1, 2;\ \lambda_\ell = 1,\ \ell = 3, 4$. Bottom: $\lambda_\ell = .1,\ \ell = 1, 2, 3, 4$. The vertices $\mathbf{v}_\ell$ are numbered counterclockwise from the origin.

e_ℓ. This proves that the map $\mathbf{T}_Q$ is one-to-one on any edge of Q. Actually, it provides a cubic reparameterization of the given edge.

Let us consider the statement $\mathbf{T}_Q(Q) = Q$. From (3.3)–(3.9) and by the convex hull property of the Bézier representation, we obtain $\mathbf{T}_Q(Q) \subset Q$ since Q is convex. To prove that $Q \subset \mathbf{T}_Q(Q)$ we proceed by contradiction. If there exists $\mathbf{p} \in Q,\ \mathbf{p} \notin \mathbf{T}_Q(Q)$, it is possible to construct a continuous map $f : Q \to \partial Q$ such that $f(\mathbf{p}) = \mathbf{p}$ for all $\mathbf{p} \in \partial Q$ (since $\mathbf{T}_Q$ is one-to-one on the boundary of Q): this contradicts Brower's theorem.

Finally, the formulas for $\mathbf{T}_Q(\mathbf{v}_\ell)$ and $J(\mathbf{T}_Q)(\mathbf{v}_\ell)$ are easily obtainable from (3.3)–(3.9). ■

By a perturbation argument, because $\mathbf{T}_Q^{(1,1,1,1)}$ is the identity map and in view of Proposition 3.2, $\mathbf{T}_Q$ is one-to-one on Q if all parameters λ_ℓ are sufficiently close to 1.

For *arbitrary* λ_ℓ we can prove this property if Q is a rectangle.

Proposition 3.3. *If Q is a rectangle and $\lambda_\ell \in (0, 1]$, $\ell = 1, 2, 3, 4$, then the transformation $\mathbf{T}_Q$ is one-to-one on Q and $\mathbf{T}_Q^{-1}$ is of class C^1.*

Proof. The partial derivatives

$$\frac{\partial X_Q}{\partial x},\ \frac{\partial X_Q}{\partial y},\ \frac{\partial Y_Q}{\partial x},\ \frac{\partial Y_Q}{\partial y}$$

are piecewise quadratic bivariate polynomials whose Bézier coefficients can be computed by standard manipulations.

For the sake of simplicity we only consider the case when Q is the unit square, where we place the first vertex $\mathbf{v}_1$ at the origin, and number all other vertices as in Fig. 1 (left). By symmetry it is sufficient to look at one subtriangle, say $T_1 = [\mathbf{v}_1, \mathbf{v}_2, \mathbf{w}]$. Using the standard notation c_{ijk} for the Bézier coefficients of a quadratic polynomial on T_1, we obtain the following expressions, where $a_\ell := 1 - \lambda_\ell$.

	$\frac{\partial X_Q}{\partial x}$	$\frac{\partial X_Q}{\partial y}$
c_{200}	$1 - a_1$	0
c_{110}	$1 + a_1 + a_2$	0
c_{020}	$1 - a_2$	0
c_{101}	$1 + a_2/2$	$(a_1 - a_4)/4$
c_{011}	$1 + a_1/2$	$(a_3 - a_2)/4$
c_{002}	$1 + (a_1 + a_2 + a_3 + a_4)/8$	$(a_1 - a_2 + a_3 - a_4)/4$

	$\frac{\partial Y_Q}{\partial x}$	$\frac{\partial Y_Q}{\partial y}$
c_{200}	0	$1 - a_1$
c_{110}	0	$1 - (a_1 + a_2)/2$
c_{020}	0	$1 - a_2$
c_{101}	$(a_1 - a_2)/4$	$1 + a_4/2$
c_{011}	$(a_1 - a_2)/4$	$1 + a_3/2$
c_{002}	$(a_1 - a_2 + a_3 - a_4)/4$	$1 + (a_1 + a_2 + a_3 + a_4)/8$

Thus, looking at the Bézier coefficients, is easy to see that for any $\lambda_\ell \in (0, 1],\ \ell = 1, 2, 3, 4$,

$$\frac{\partial X_Q}{\partial x} > \left|\frac{\partial X_Q}{\partial y}\right|, \qquad \frac{\partial Y_Q}{\partial y} > \left|\frac{\partial Y_Q}{\partial x}\right|$$

at any point of Q. Therefore the Jacobian of the transformation $\mathbf{T}_Q$ diagonally dominant and hence nonsingular at any point. In view of Proposition 3.2 this implies that $\mathbf{T}_Q$ is invertible because it is proper, locally invertible and invertible on the boundary, see e.g. [1]. Finally, $\mathbf{T}_Q^{-1}$ is of class C^1 since $\mathbf{T}_Q$ is C^1 and its Jacobian is nonsingular. ■

Remark 3.1. We conjecture that $J(\mathbf{T}_Q)$ is nonsingular in Q for any convex quadrialteral Q and any choice of $\lambda_\ell \in (0, 1]$. However, the case of a rectangle is already useful for scattered data fitting applications, see the examples in Section 5.

Assuming that $\mathbf{T}_Q$ is a one-to-one map of the quadrilateral Q, the graph of $\mathbf{S}_Q$ is the graph of a bivariate function $s_Q = Z_Q \circ \mathbf{T}_Q^{-1}$. That is, by setting

$$(x, y)^T = \mathbf{T}_Q^{(\lambda_1,\lambda_2,\lambda_3,\lambda_4)}(\tilde{x}, \tilde{y}),$$

the invertibility of the map $\mathbf{T}_Q$ allows us to define a function $s_Q : Q \to \mathbb{R}$ by

$$s_Q(x, y) = s_Q^{(\lambda_1,\lambda_2,\lambda_3,\lambda_4)}(x, y) := Z_Q^{(\lambda_1,\lambda_2,\lambda_3,\lambda_4)}(\tilde{x}, \tilde{y}), \qquad (x, y) \in Q. \tag{3.12}$$

It is easy to see that s_Q interpolates the data (2.2), i.e.,

$$s_Q(\mathbf{v}_\ell) = f_{\mathbf{v}_\ell}, \quad \nabla s_Q(\mathbf{v}_\ell) = \nabla f_{\mathbf{v}_\ell}, \qquad \ell = 1, 2, 3, 4. \tag{3.13}$$

Indeed, by (3.3) $s_Q(\mathbf{v}_\ell) = Z_Q \circ \mathbf{T}_Q^{-1}(\mathbf{v}_\ell) = Z_Q(\mathbf{v}_\ell) = f_{\mathbf{v}_\ell}$. Furthermore, from (3.3)–(3.8) it follows that $\nabla Z_Q(\mathbf{v}_\ell) = \lambda_\ell \nabla f_{\mathbf{v}_\ell}$, and hence by Proposition 3.2 we have at $\mathbf{v}_\ell$

$$\nabla s_Q = \nabla Z_Q \cdot J(\mathbf{T}_Q)^{-1} = \lambda_\ell \nabla f_{\mathbf{v}_\ell} \begin{bmatrix} \lambda_\ell & 0 \\ 0 & \lambda_\ell \end{bmatrix}^{-1} = \nabla f_{\mathbf{v}_\ell}$$

as soon as $\lambda_\ell > 0$.

By patching together the tensioned macro-elements s_Q, $Q \in \square$, we obtain a function $s^\Lambda : \Omega \to \mathbb{R}$,

$$s^\Lambda|_Q := s_Q, \quad Q \in \square,$$

whose graph is also given by the surface $\mathbf{S}^\Lambda$.

Let us consider the smoothness of s^Λ, see also [23]. Clearly, in case that all $\mathbf{T}_Q$, $Q \in \square$, are invertible, we have $s^\Lambda = Z^\Lambda \circ (\mathbf{T}^\Lambda)^{-1}$, where

$$\mathbf{T}^\Lambda(x, y) = (X^\Lambda(x, y), Y^\Lambda(x, y))^T,$$

and

$$(\mathbf{T}^\Lambda)^{-1}|_Q = \mathbf{T}_Q^{-1}, \quad Q \in \square.$$

As mensioned above, $X^\Lambda, Y^\Lambda, Z^\Lambda$ are C^1 functions on Ω, which already implies that s^Λ is a continuous function. Assuming in addition that the Jacobians of all $\mathbf{T}_Q$ are nonsingular, we conclude that $(\mathbf{T}^\Lambda)^{-1}$ is a C^1 mapping on Ω, which implies that $s^\Lambda \in C^1(\Omega)$ in this case, which happens in particular when all $Q \in \square$ are rectangles and $\lambda_{\mathbf{v}} > 0$ for all $\mathbf{v} \in \mathcal{V}$, according to Proposition 3.3. Fig. 3 illustrates the smooth patching of the macro-elements s_Q together.

Summarizing, we have obtained the following result.

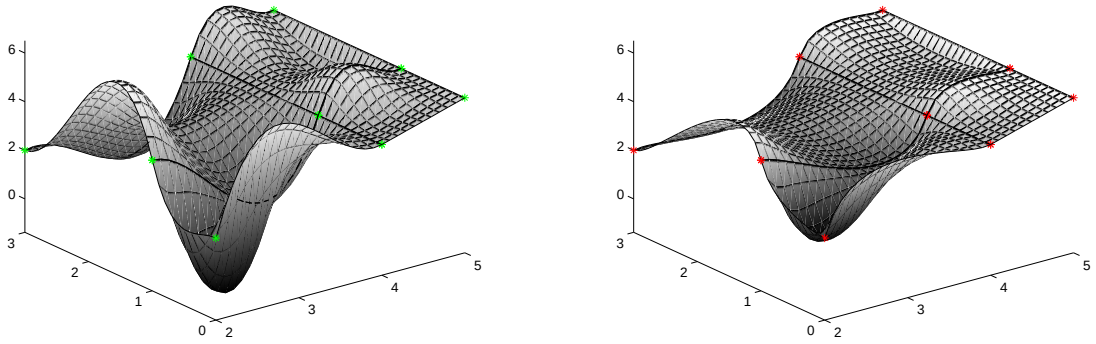

Figure 3: Four tensioned FVS elements patched together: Left: $\lambda_\ell = 1$,. Right: $\lambda_\ell = .4$.

Theorem 3.4. *Given any $\lambda_{\mathbf{v}} \in (0,1]$, $\mathbf{v} \in \mathcal{V}$, assume that the Jacobian of each mapping $\mathbf{T}_Q$, $Q \in \square$, is nonsingular in Q. (This is always the case if Q is a rectangle.) Then the tensioned FVS spline s^Λ is well defined as a function in $C^1(\Omega)$. Moreover, s^Λ interpolates the given values $f_{\mathbf{v}}$ and gradients $\nabla f_{\mathbf{v}}$ of the corresponding FVS spline s at all vertices of $\square$. In the case that $\lambda_{\mathbf{v}} = 1$, $\mathbf{v} \in \mathcal{V}$, s^Λ coincides with s. If all $\lambda_{\mathbf{v}} \to 0$, then s^Λ converges to a continuous surface whose restriction to any $Q = [\mathbf{v}_1, \mathbf{v}_2, \mathbf{v}_3, \mathbf{v}_4] \in \square$ has the properties described in Proposition 3.1, in particular its graph is contained in the convex hull of the four points $(\mathbf{v}_\ell, f_{\mathbf{v}_\ell})^T$, $\ell = 1, 2, 3, 4$.*

Remark 3.2. If $s \in S_3^1(\boxtimes)$ is a polynomial of first degree on $Q \in \square$, then it follows from (3.3)-(3.9) that the Bézier control points $\mathbf{C}_{i,j,k}^{T_\ell}$ belong to the plane which is the graph of $s|_Q$, and the same does $\mathbf{S}_Q$ due to the properties of Bézier-Bernstein representation. So, the two functions s_Q and $s|_Q$ have the same graph. That is, s^Λ locally reproduces first degree polynomials. This property can be used to prove second order error estimates for the interpolation with the tensioned FVS spline, see [23].

Remark 3.3. The parametric tension approach has been applied previously to the cubic Clough-Tocher and quadratic Powell-Sabin macro-elements, obtaining tensioned macro-elements reproducing first degree polynomials as well, see [5, 23]. An advantage of the scheme presented here over the tensioned Powell-Sabin element is the higher approximation order of the underlying macro-element (h^4 versus h^3), which allows more economical representation of smoother parts of the surface *before* tension parameters are chosen. On the other hand, comparing to the tensioned Clough-Tocher element of [5], our FVS element is guaranteed to be given by a function for all values of the tension parameters, at least in the case of a rectangular partition, rather than for the values of $\lambda_{\mathbf{v}}$ is a neighborhood of 1 or 0. See [23] for a comparison to different tension techniques, in particular those of [2]. Finally, since our main theoretical results hold for a uniform type triangulation, it is worth emphasizing that the action of the tension parameters for the FVS element is completely local, in contrast to standard tension methods based on tensor-product structures where the tension parameters have to be assigned to the grid lines going through the whole domain. For the sake of completeness, we mention that such a local control could also be obtained by the parametric cubic Coons patches presented in [4]. Nevertheless, the construction in [4] is significantly more involved than the one presented here since it builds on bicubic functions instead of piecewise cubics. Careful numerical comparison of various tension techniques combined with scattered data fitting is left for future research.

Remark 3.4. A reduced FVS macro-element (with approximation order h^3) has been used in [15] to construct a C^1 monotone piecewise cubic interpolant to monotone data, where the monotonicity is required in both variables simultaneously, following [3]. The approaches to shape preservation presented here and in [15] possess certain similarity, as in [15] the monotonicity of the constructed surface is achieved by suitably reducing the size of the *initial gradient values* at the data sites, whereas in our scheme the *gradients of the parametric components* are reduced to achive monotonicity, convexity or prescribed local bounds on the surface, see Section 4 below. Apart from a greater flexibility (various shape preserving goals can be achieved, not only monotonicity), the advantages of the scheme presented here include the exact interpolation of the gradients and, once again, the higher approximation order of the underlying macro-element.

4 Selection of tension parameters

The parameters λ_ℓ act as shape/tension parameters on the function s_Q, thus they can be selected to (automatically) control its shape. In particular, we can obtain shape preservation on the edges of the FVS quadrilateral by using univariate selection of tension parameters if the data is monotone and/or convex.

Assume that the data is *monotone along the edge* $\mathbf{e}_\ell$ that is the quantities

$$f_{\mathbf{v}_{\ell+1}} - f_{\mathbf{v}_\ell},\ \langle \nabla f_{\mathbf{v}_\ell}, \mathbf{e}_\ell \rangle,\ \langle \nabla f_{\mathbf{v}_{\ell+1}}, \mathbf{e}_\ell \rangle$$

are either all positive or they are all negative.

Clearly, s_Q is monotone along the same edge if and only if $Z_Q|_{\mathbf{e}_\ell}$ (see (3.10)) is monotone (see Proposition 3.2). Since $Z_Q|_{\mathbf{e}_\ell}$ is a cubic polynomial interpolating the data

$$f_{\mathbf{v}_\ell},\ f_{\mathbf{v}_{\ell+1}},\ \lambda_\ell \langle \nabla f_{\mathbf{v}_\ell}, \frac{\mathbf{e}_\ell}{\|\mathbf{e}_\ell\|} \rangle,\ \lambda_{\ell+1} \langle \nabla f_{\mathbf{v}_{\ell+1}}, \frac{\mathbf{e}_\ell}{\|\mathbf{e}_\ell\|} \rangle$$

it is well known, [13], that a sufficient condition to ensure its monotonicity is given by

$$\max \left\{ \lambda_\ell \langle \nabla f_{\mathbf{v}_\ell}, \frac{\mathbf{e}_\ell}{\|\mathbf{e}_\ell\|} \rangle,\ \lambda_{\ell+1} \langle \nabla f_{\mathbf{v}_{\ell+1}}, \frac{\mathbf{e}_\ell}{\|\mathbf{e}_\ell\|} \rangle \right\} \leq 3 \frac{f_{\mathbf{v}_{\ell+1}} - f_{\mathbf{v}_\ell}}{\|\mathbf{e}_\ell\|}.$$

Thus it suffices to select $\lambda_\ell, \lambda_{\ell+1}$ such that

$$\lambda_\ell \leq \min \left\{ 1,\ 3 \frac{f_{\mathbf{v}_{\ell+1}} - f_{\mathbf{v}_\ell}}{\langle \nabla f_{\mathbf{v}_\ell}, \mathbf{e}_\ell \rangle} \right\},\ \lambda_{\ell+1} \leq \min \left\{ 1,\ 3 \frac{f_{\mathbf{v}_{\ell+1}} - f_{\mathbf{v}_\ell}}{\langle \nabla f_{\mathbf{v}_{\ell+1}}, \mathbf{e}_\ell \rangle} \right\}. \tag{4.1}$$

Remark 4.1. If Q is a rectangle, by standard manipulation on partial derivatives of Z_Q it turns out that in the limit case $\lambda_\ell = 0,\ \ell = 1, 2, 3, 4$ the derivative

$$\frac{\partial Z_Q}{\partial \mathbf{e}_\ell},$$

is a bivariate quadratic polynomial whose Bézier coefficients are non negative if the data is increasing along both $\mathbf{e}_\ell$ and $-\mathbf{e}_{\ell+2}$. Thus, in the limit case Z_Q is monotone increasing along directions parallel to the edge $\mathbf{e}_\ell$ and the same holds true for s_Q. In any fixed compact subset of Q, s_Q retains the same behavior for sufficiently small values of the shape parameters.

Similarly, assume the data is *convex along the edge* $\mathbf{e}_\ell$, that is

$$\langle \nabla f_{\mathbf{v}_\ell}, \mathbf{e}_\ell \rangle < f_{\mathbf{v}_{\ell+1}} - f_{\mathbf{v}_\ell} < \langle \nabla f_{\mathbf{v}_{\ell+1}}, \mathbf{e}_\ell \rangle.$$

The graph of s_Q along the same edge is the support of the planar parametric cubic curve $\mathbf{S}_Q|_{\mathbf{e}_\ell}$. Thus, s_Q is convex along $\mathbf{e}_\ell$ if and only if the curvature of this cubic curve is nonnegative that is if and only if, [18],

$$\left[(\mathbf{C}^{T_\ell}_{2-j,j+1,0} - \mathbf{C}^{T_\ell}_{3-j,j,0}) \times (\mathbf{C}^{T_\ell}_{1-j,j+2,0} - \mathbf{C}^{T_\ell}_{2-j,j+1,0})\right] \cdot (\mathbf{e}_\ell \times \mathbf{k}) \geq 0,\ \ j = 0, 1.$$

where $\mathbf{a}\times\mathbf{b}$ denotes the vector product between $\mathbf{a}$ and $\mathbf{b}$, and $\mathbf{k} = (0, 0, 1)^T$. From (3.2)–(3.9) the previous inequalities read

$$f_{\mathbf{v}_{\ell+1}} - f_{\mathbf{v}_\ell} - \frac{\lambda_\ell}{3}\langle \nabla f_{\mathbf{v}_\ell}, \mathbf{e}_\ell\rangle - \frac{\lambda_{\ell+1}}{3}\langle \nabla f_{\mathbf{v}_{\ell+1}}, \mathbf{e}_\ell\rangle \geq \left[1 - \frac{\lambda_\ell}{3} - \frac{\lambda_{\ell+1}}{3}\right]\langle \nabla f_{\mathbf{v}_\ell}, \mathbf{e}_\ell\rangle$$
$$f_{\mathbf{v}_{\ell+1}} - f_{\mathbf{v}_\ell} - \frac{\lambda_\ell}{3}\langle \nabla f_{\mathbf{v}_\ell}, \mathbf{e}_\ell\rangle - \frac{\lambda_{\ell+1}}{3}\langle \nabla f_{\mathbf{v}_{\ell+1}}, \mathbf{e}_\ell\rangle \leq \left[1 - \frac{\lambda_\ell}{3} - \frac{\lambda_{\ell+1}}{3}\right]\langle \nabla f_{\mathbf{v}_{\ell+1}}, \mathbf{e}_\ell\rangle$$

that is

$$f_{\mathbf{v}_{\ell+1}} - f_{\mathbf{v}_\ell} - \langle \nabla f_{\mathbf{v}_\ell}, \mathbf{e}_\ell\rangle \geq \frac{\lambda_{\ell+1}}{3}\left[\langle \nabla f_{\mathbf{v}_{\ell+1}}, \mathbf{e}_\ell\rangle - \langle \nabla f_{\mathbf{v}_\ell}, \mathbf{e}_\ell\rangle\right]$$
$$f_{\mathbf{v}_{\ell+1}} - f_{\mathbf{v}_\ell} - \langle \nabla f_{\mathbf{v}_{\ell+1}}, \mathbf{e}_\ell\rangle \leq \frac{\lambda_\ell}{3}\left[\langle \nabla f_{\mathbf{v}_\ell}, \mathbf{e}_\ell\rangle - \langle \nabla f_{\mathbf{v}_{\ell+1}}, \mathbf{e}_\ell\rangle\right]$$

Thus, s_Q is convex along the edge $\mathbf{e}_\ell$ if and only if

$$\begin{aligned}
\lambda_\ell &\leq \min\left\{1,\ 3\frac{\langle \nabla f_{\mathbf{v}_{\ell+1}}, \mathbf{e}_\ell\rangle - [f_{\mathbf{v}_{\ell+1}} - f_{\mathbf{v}_\ell}]}{\langle \nabla f_{\mathbf{v}_{\ell+1}}, \mathbf{e}_\ell\rangle - \langle \nabla f_{\mathbf{v}_\ell}, \mathbf{e}_\ell\rangle}\right\} \\
\lambda_{\ell+1} &\leq \min\left\{1,\ 3\frac{[f_{\mathbf{v}_{\ell+1}} - f_{\mathbf{v}_\ell}] - \langle \nabla f_{\mathbf{v}_\ell}, \mathbf{e}_\ell\rangle}{\langle \nabla f_{\mathbf{v}_{\ell+1}}, \mathbf{e}_\ell\rangle - \langle \nabla f_{\mathbf{v}_\ell}, \mathbf{e}_\ell\rangle}\right\}.
\end{aligned} \tag{4.2}$$

Finally, in view of Proposition 3.1, it is always possible to *prescribe local bounds* on the tensioned surface by choosing parameters $\lambda_\ell > 0$, $\ell = 1, 2, 3, 4$, such that

$$m_Q \leq s_Q(x, y) \leq M_Q, \qquad (x, y) \in Q, \tag{4.3}$$

provided m_Q and M_Q are any given bounds satisfying

$$m_Q < \min\{f_{\mathbf{v}_1}, f_{\mathbf{v}_2}, f_{\mathbf{v}_3}, f_{\mathbf{v}_4}\}, \quad \max\{f_{\mathbf{v}_1}, f_{\mathbf{v}_2}, f_{\mathbf{v}_3}, f_{\mathbf{v}_4}\} < M_Q.$$

This is useful in particular for removing undesired local minima and maxima. The exact conditions on $\lambda_{\mathbf{v}}$ that guarantee (4.3) can be easily worked out using the formulas (3.3)–(3.9) and requiring that the Bézier coefficients $c_{\mathbf{t}}$, $\mathbf{t} \in \mathcal{D}_Q$, satisfy the same double inequality.

5 Application to Scattered Data Fitting

The idea of tension is used extensively in practical scattered data fitting algorithms to eliminate artificial oscillations and extraneous inflection points often arising in the undersampled areas with strong changes in the surface gradient or curvature, see e.g. [25, 26], where a tension parameter is introduced into the minimum curvature surfaces.

Our approach allows to apply tension to piecewise cubic surfaces generated by the recent two-stage method of scattered data fitting [8, 14, 6, 7, 9] based on the extension of local approximations to a spline in $S^1_3(\boxtimes)$. As demonstrated in the above cited references, this method is fast and robust and capable to produce high quality surfaces from difficult terrain

data with strong variations in data density. Still, small scale artifacts can occur in most difficult areas, as exemplified in Fig. 4 that represents an FVS spline computed for the Black Forest data described in detail in [8] and available with the software package TSFIT [9]. The parameters of the two-stage method are the same as those used in [8, Section 6.6], with the exception that we are using in the second stage the operator Q_1^{av} leading to a spline in $S_3^1(\boxtimes)$ rather than RQ_2^{av} which produces a C^2 sextic spline.

Note that the local approximation with radial basis functions used in [6, 7] has led to surfaces with significantly weaker artifacts, but we have chosen this example to emphasize the effect of tension. By the same reason we have not preprocessed the data $f_{\mathbf{v}}, \nabla f_{\mathbf{v}}$ produced by the scattered data fitting algorithm by any filtering or smoothing techniques, even though this could bring a further reduction of the artifacts.

Recall that we assign tension parameters $\lambda_{\mathbf{v}}$ to all vertices $\mathbf{v}$ of the quadrangulation $\square$. Therefore the question of automatic selection of these parameters must be addressed. Indeed, an advantage of having a spatially distributed sequence of parameters is that it can be adjusted to the local behaviour of the surface. As apparent from Fig. 4, the artifacts occur in the flat terrain with extremely few data and especially in the transition regions between the flat areas and steeper areas with higher data density. Therefore we leave the spline surface unchanged in the regions of high slope by setting

$$\lambda_{\mathbf{v}} = 1 \quad \text{whenever} \quad \text{slope}(\mathbf{v}) > 0.05, \tag{5.1}$$

where

$$\text{slope}(\mathbf{v}) := \max\Big\{ \frac{|f_{\mathbf{w}} - f_{\mathbf{v}}|}{\|\mathbf{w} - \mathbf{v}\|} \ : \ \mathbf{w} \text{ is connected to } \mathbf{v} \text{ by an edge of } \square \Big\}.$$

We also avoid making tension too severe, because, as explained above, for very small values of $\lambda_{\mathbf{v}}$ the tensioned surface becomes linear along the edges of $\square$. Clearly, this may create artifacts itself. Therefore we ensure that

$$\lambda_{\mathbf{v}} > 0.15 \quad \text{for all} \quad \mathbf{v} \in \mathcal{V}. \tag{5.2}$$

Within the constraints (5.1) and (5.2), we choose for each $\lambda_{\mathbf{v}}$ the greatest possible value such that the monotonicity condition (4.1) is satisfied for each edge $\mathbf{e} \in \mathcal{E}$ attached to $\mathbf{v}$ such that the data is monotone along it, and the convexity condition (4.2) is satisfied for each edge $\mathbf{e} \in \mathcal{E}$ attached to $\mathbf{v}$ such that the data is convex along it.

Figs 5 and 6 demonstrate the improvements in the surface shape obtained by applying this algorithm. Fig. 5 depicts the tensioned surface visualized from the same viewpoint that the original spline surface in Fig. 4, whereas Fig. 6 provides a comparison of the contour lines produced using fine grid evaluations of both surfaces. The figures confirm a substantial reduction of artificial oscillations in the tensioned surface.

We conclude this section by mentioning that the evaluation of the tensioned surface at a prescribed point $(x, y) \in Q$, $Q \in \square$ requires the inversion of the transformation $\mathbf{T}_Q$, see (3.12), that is the solution of a nonlinear system described by two piecewise cubic functions. Since the quadrangulations used in [8] consist of squares, Proposition 3.3 guarantees that the unique solution is available for any choice of the tension parameters. Due to the Bézier representation, the Jacobian of the transformation can be efficiently computed using the formulas in the proof of Proposition 3.3, and the solution of the nonlinear system can be efficiently approximated by using the Newton method. It turns out that, considering as starting point the pair (x, y) itself (corresponding to the exact solution if $\lambda_v = 1$), very few iterations of the method provide an accurate approximation of the solution. Of course, the closer to 1 are the tension parameters associated to the vertices of Q, the more efficient is the process. The average number of iterations needed to achieve 14 digits accuracy increases

from 1 for $\lambda_v \approx 1$ to 8 for $\lambda_v = 0.5$ and 10 for $\lambda_v \approx 0$. The cputime per evaluation increases with a factor of about 3. (Clearly, this figure is implementation-dependent.) The average number of iterations per evaluation for the surface in Figs 5 and 6 is about 2.6.

6 Conclusion

We have presented a method, based on the parametric approach [22, 5, 23], to produce C^1 surfaces with tension properties interpolating a given set of Hermite data at the vertices of a quadrangulation $\square$. The method constructs the interpolating function as a particular parametric surface having C^1 piecewise cubic components, where each component is obtained according to the FVS cubic macro-element construction.

Each vertex of the quadrangulation is equipped with a parameter which acts as a tension parameter "stretching" the graph of the obtained surface around the vertex itself. Each parameter has a local effect in the sense that it influences the shape of the surface only in the four quadrilaterals sharing the corresponding vertex.

Automatic methods for selection of the tension parameters ensuring monotonicity and/or convexity preservation along the edges of the quadrilaterals have been presented.

It is worth to notice that the evaluation of the obtained surface at a prescribed point requires the inversion of a piecewise cubic transformation, which can be efficiently achieved by means of a few iterations of the Newton method.

The application of the proposed method to scattered data fitting allows to remove artifacts and easily control the shape of the obtained surface.

Acknowledgement. We are grateful to London Mathematical Society for the financial support of a visit by the second named author to the University of Strathclyde in the Spring of 2007, which helped us to start collaboration on the subject of this research.

References

[1] A. Ambrosetti and G. Prodi, *A Primer of Nonlinear Analysis*, Cambridge University Press, Cambridge, UK, 1993.

[2] P. Costantini, Curve and surface construction using variable degree polynomial splines, *Comput. Aided Geom. Design* **24** (2000), 426-446.

[3] R. E. Carlson and F. N. Fritsch, Monotone piecewise bicubic interpolation, *SIAM J. Numer. Anal.* **22** (1985), 386–400.

[4] P. Costantini and C. Manni, Comonotone parametric C^1 interpolation of non-gridded data, *J. Comput. Applied. Math.* **75** (1996), 147–169.

[5] P. Costantini and C. Manni, A parametric cubic element with tension properties, *SIAM J. Numer. Anal.* **36** (1999), 607–628.

[6] O. Davydov, R. Morandi and A. Sestini, Local hybrid approximation for scattered data fitting with bivariate splines, *Comput. Aided Geom. Design* **23** (2006), 703–721.

[7] O. Davydov, A. Sestini and R. Morandi, Local RBF approximation for scattered data fitting with bivariate splines, *in* "Trends and Applications in Constructive Approximation," (M. G. de Bruin, D. H. Mache, and J. Szabados, Eds.), ISNM Vol. 151, Birkhäuser, 2005, pp. 91–102.

[8] O. Davydov and F. Zeilfelder, Scattered data fitting by direct extension of local polynomials to bivariate splines, *Advances in Comp. Math.* **21** (2004), 223–271.

[9] O. Davydov and F. Zeilfelder, TSFIT: A Software Package for Two-Stage Scattered Data Fitting, 2005, available under GPL from
`http://www.maths.strath.ac.uk/~aas04108/tsfit/`

[10] R. Delbourgo and J.A. Gregory Shape preserving piecewise rational interpolation, *SIAM J. Sci. Stat. Comput.* **6** (1985), 967–976.

[11] A. Edelman and C. A. Micchelli, Admissible slopes for monotone and convex interpolation, *Numer. Math.* **51** (1987), 441-458.

[12] B. Fraeijs de Veubeke, A conforming finite element for plate bending, *J. Solids Structures* **4** (1968), 95–108.

[13] F.N. Fritsch and R.E. Carlson, Monotone piecewise cubic interpolation, *SIAM J. Numer. Anal.* **17** (1980), 238–246.

[14] J. Haber, F. Zeilfelder, O. Davydov and H.-P. Seidel, Smooth approximation and rendering of large scattered data sets, *IEEE Visualization 2001*, pp. 341–347, 571.

[15] L. Han and L. L. Schumaker, Fitting monotone surfaces to scattered data using C^1 piecewise cubics, *SIAM J. Numer. Anal.* **34** (1997), 569-585.

[16] G. Sander, Bornes supérieures et inférieures dans l'analyse matricielle des plaques en flexion-torsion, *J. Bull. Soc. Royale Sciences Liège* **33** (1964), 456–494.

[17] T.N.T. Goodman, Shape preserving interpolation by curves. In: J. Levesley, I. J.Anderson and J. C. Mason, eds., Algorithms for Approximation IV, (2002) pp. 24–35, Huddersfield: University of Huddersfield Proceedings.

[18] J. Hoschek and D. Lasser, Fundamentals of Computer Aided Geometric Design, A. K. Peters, Wellesley, Massachusetts, 1993.

[19] P.E. Koch, T. Lyche, Interpolation with exponential B-splines in tension, in G. Farin et al. eds., Geometric modelling, *Comput.* Suppl. 8 (1993), 173–190. Berlin: Springer-Verlag.

[20] B.I. Kvasov, Algorithms for shape preserving local approximation with automatic selection of tension parameters, *Comput. Aided Geom. Design* **17** (2000), 17–37.

[21] M.-J. Lai and L. L. Schumaker, Spline Functions on Triangulations, Cambridge University Press, Cambridge, 2007.

[22] C. Manni, C^1 comonotone Hermite interpolation via parametric cubics, *J. Comput. Applied. Math.* **69** (1996), 143–157.

[23] C. Manni: A general parametric framework for functional tension schemes, *J. Comput. Applied. Math.* **119** (2000), 275-300.

[24] D.G. Schweikert, An interpolation curve using a spline in tension, *J. Math. Phys.* **45** (1966), 312–317.

[25] W. H. F. Smith and P. Wessel, Gridding with continuous curvature splines in tension, *Geophysics* **55** (1990), 293–305.

[26] W. H. F. Smith and P. Wessel, GMT - The Generic Mapping Tools, http://gmt.soest.hawaii.edu/

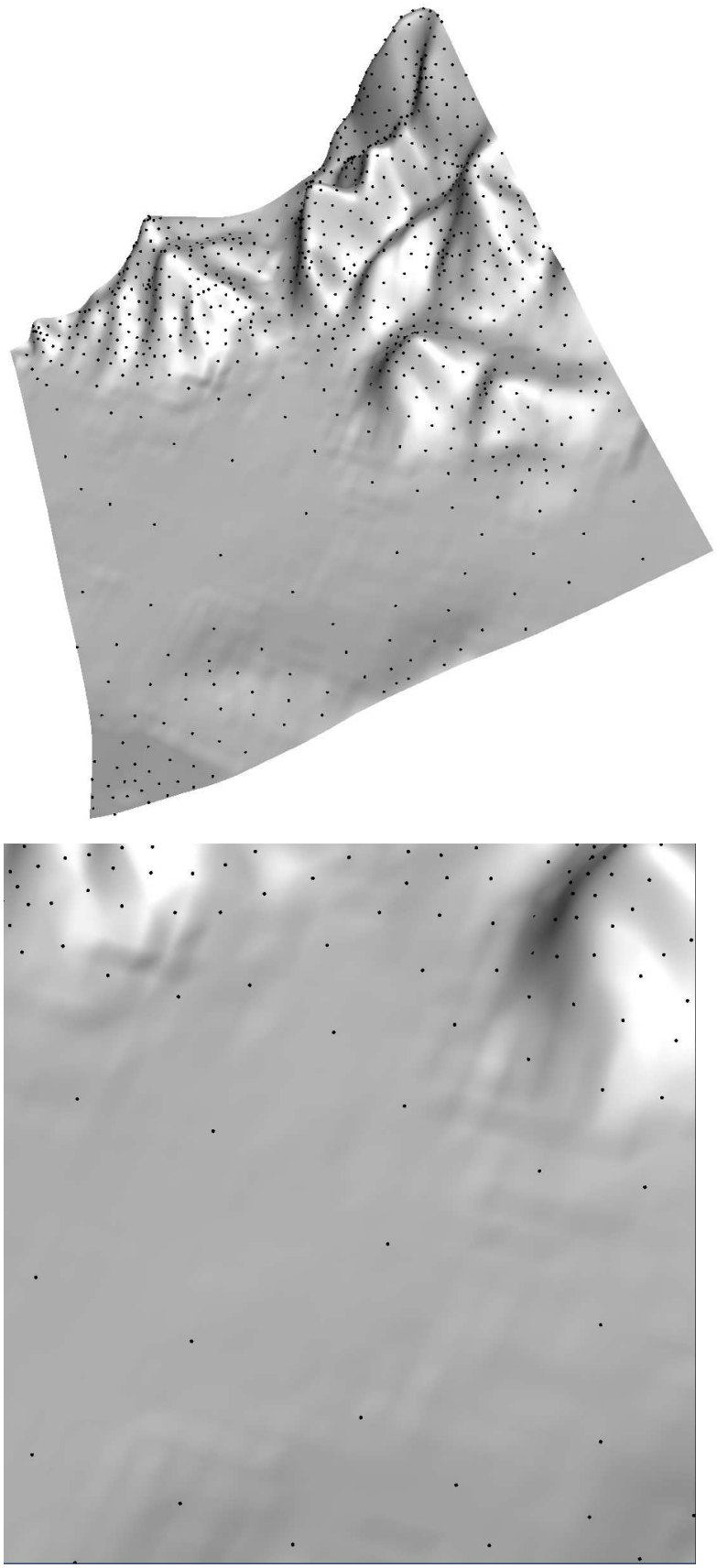

Figure 4: FVS spline surface computed from scattered data (Black Forest data set) by the two-stage method of [8], and a zoom showing small scale artifacts in a flat region. The small dots represent the data.

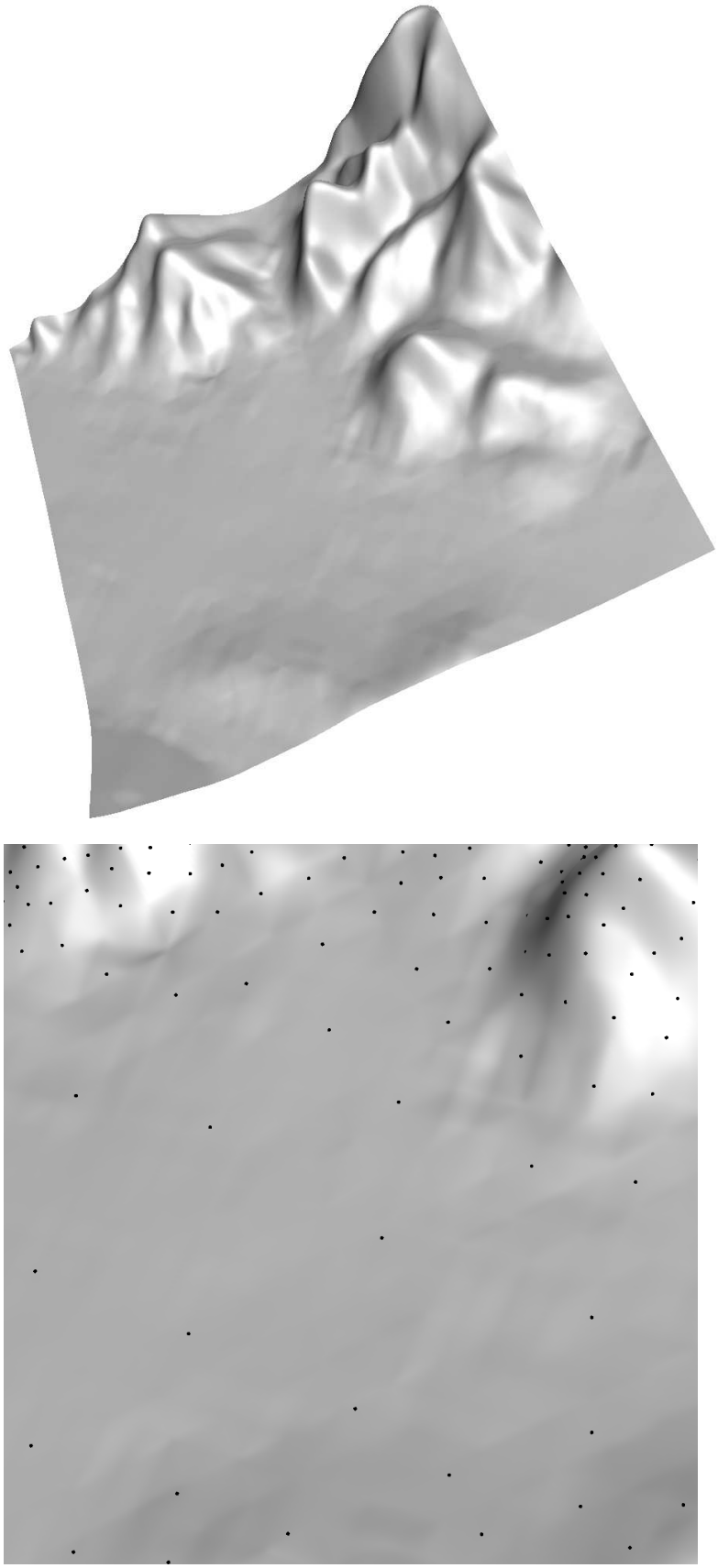

Figure 5: Tensioned surface obtained from the spline depicted in Fig. 4 by applying the algorithm described in Section 5. The artefacts are significantly reduced.

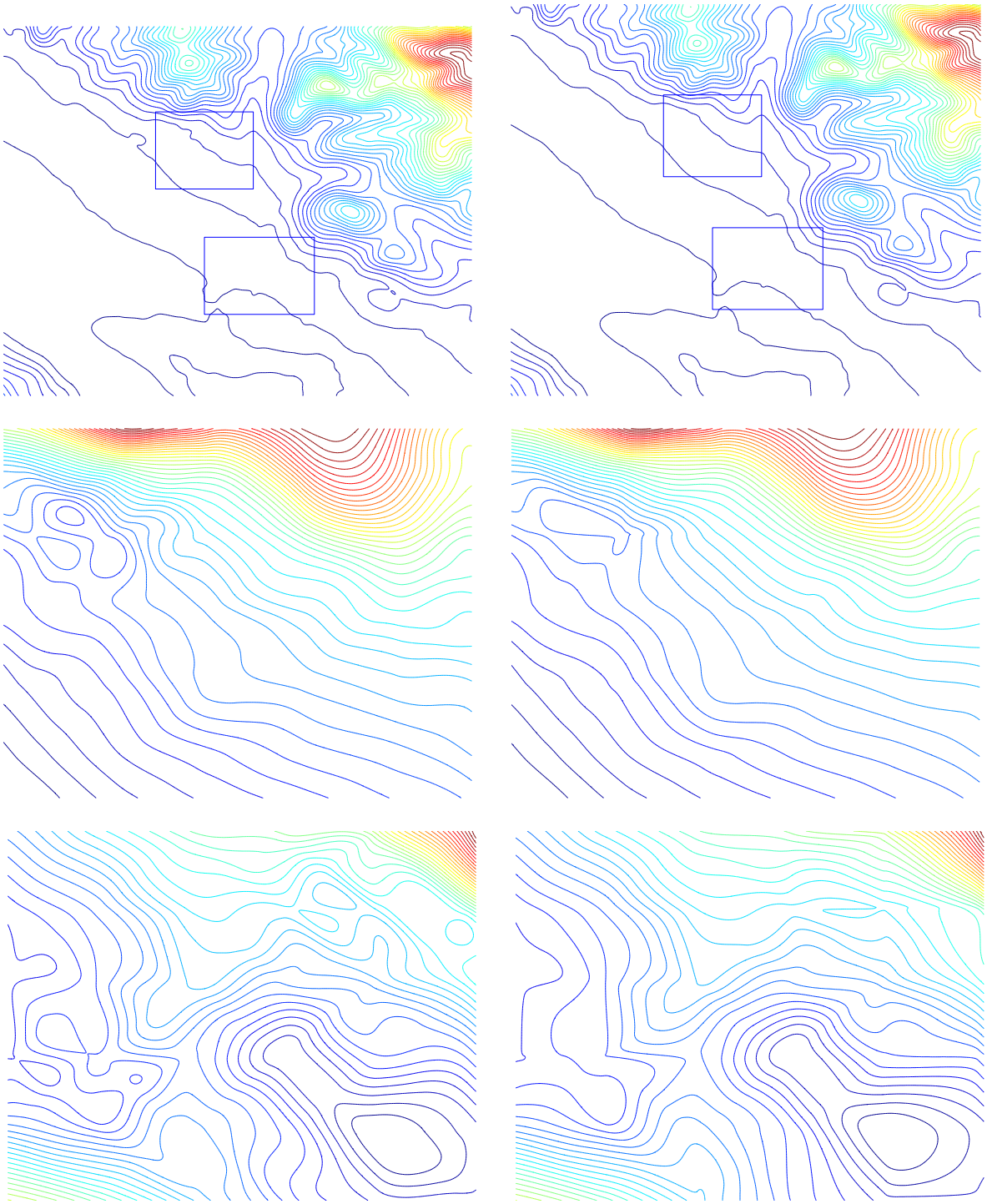

Figure 6: Contour lines of the spline surface (left) and its tensioned counterpart (right). Top: the contour lines in the the region depicted in Figs 4 (left) and 5 (left). Middle and bottom: contour lines in the sub-regions indicated by two boxes in the top figures.